

Microstructure and phase composition of as-cast Mg–9Er–6Y–xZn–0.6Zr alloys

Jing-feng WANG^{1,2}, Peng-fei SONG¹, Fu-sheng PAN^{1,2}, Xiao-en ZHOU¹

1. College of Materials Science and Engineering, Chongqing University, Chongqing 400044, China;

2. National Engineering Research Center for Magnesium Alloys, Chongqing University, Chongqing 400044, China

Received 9 January 2012; accepted 19 September 2012

Abstract: The microstructure and phase composition of as-cast Mg–9Er–6Y–xZn–0.6Zr ($x=1, 2, 3, 4$; normal mass fraction in %) alloys were investigated. In low Zn content, aside from the major second phase of Mg₂₄(Er, Y, Zn)₅, there are a few lamellar phases that grow parallel with each other from the grain boundaries to the grain interior. With Zn content increasing, the Mg₂₄(Er, Y, Zn)₅ phase decreases, but the Mg₁₂Zn(Y, Er) phase and lamellar phases continuously increase. When Zn content reaches 4% (normal mass fraction), the Mg₁₂Zn(Y, Er) phase mainly exists as large bulks, and some α -Mg grains are thoroughly penetrated by the lamellar phases. Moreover, the crystallography structures of the Mg₁₂Zn(Y, Er) and Mg₂₄(Er, Y, Zn)₅ phases are confirmed as 18R-type long-period stacking ordered structure and body-centred cubic structure, respectively.

Key words: magnesium alloys; microstructure; phase composition; long-period stacking ordered (LPSO) structure phase

1 Introduction

Recently, there has been increasing interest in the use of magnesium alloys with rare-earth (RE) elements, due to their good mechanical properties and remarkable precipitation hardening effect by aging [1–6]. Four kinds of stacking sequences in LPSO structures (i.e., 10H, 14H, 18R, and 24R) have been discovered in rapidly solidified Mg₉₇Zn₁Y₂ (mole fraction, %) alloy [7]. In Mg–8Y–2Zn–0.6Zr (mass fraction, %) alloy, ZHU et al [8] have found that the 18R structure has the chemical composition of Mg₁₀Y₁Zn₁, but not Mg₁₂Y₁Zn₁ (as commonly accepted in literature). Mg₁₂Y₁Zn₁ is actually the composition of the 14H structure, which is identical with that of the equilibrium X-phase reported in Mg–Y–Zn systems.

Another study [9] has combined the heavy RE element Gd with the light RE element Y in the Mg–8.8Gd–3.1Y–0.6Zn–0.5Zr (mass fraction, %) alloy that presents an ultimate tensile strength (UTS) of 430 MPa and tensile yield strength of 375 MPa attained by extrusion and aging at 200 °C for 63 h. HOMMA et al [10] have successfully fabricated the extraordinarily

high-strength Mg–1.8Gd–1.8Y–0.7Zn–0.2Zr (mole fraction, %) alloy which has a UTS of 542 MPa, proof stress of 473 MPa, and elongation to failure of 8.0%.

In the Mg–Zn–Y and Mg–Zn–Er systems, the LPSO phase forms as a secondary phase in the grain boundaries during solidification. The LPSO structure is 18R, and mainly changes to 14H with high-temperature annealing [11,12]. The 18R-type LPSO structure is also found in the Mg₉₇Zn₁Er₂ (mole fraction, %) alloy prepared by the induction melting method, and its average composition is Mg–7Zn–5Er (mole fraction, %), as estimated by energy dispersive X-ray spectrometry (EDS) [10]. The face-centered icosahedral quasi-crystalline phase (*I*-phase) and face-centered cubic structure *W*-phase coexist in the Mg–5Zn–2.5Er (mass fraction, %) alloy [13] and the *I*-phase precipitates after solution treatment at 440 °C for 10 h [14]. ZHANG et al [15] have also found that the addition of the RE element Er significantly leads to a clear yielding in tensile curves. After extrusion at 420 °C, the 1% Er-containing alloy exhibits the best ultimate (305 MPa) and yield (285 MPa) strengths, with a large tensile elongation of 25% [16].

Indeed, the effects of trace Er addition on the

microstructure and mechanical properties of Mg–Zn–Er alloys have been extensively studied. However, investigations on the microstructure and phase composition of Mg alloys with Er as the major alloy element are limited by now. The Er atom has almost similar physical properties with the Gd atom. There have been many studies on Mg–Gd–Y–Zn–Zr alloys. Nevertheless, research on the Mg–Er–Y–Zn–Zr alloy using Er as a substitute for Gd has not yet been conducted. In the present work, Mg–9Er–6Y– x Zn–0.6Zr ($x=1, 2, 3, 4$; normal mass fraction in %) series alloys were prepared in an electromagnetic induction furnace with the heavy RE element Er as the major alloying element, combined with the light RE element Y and different Zn contents. Changes in the microstructure and phase composition of these alloys with different Zn contents were investigated by optical microscopy, X-ray diffraction (XRD), scanning electron microscopy (SEM) and EDS.

2 Experimental

The starting materials were commercial Mg (99.95% purity), Zn (99.95% purity), as well as Mg–30Zr, Mg–25Y, and Mg–25Er master alloys. From these materials, experimental Mg–9Er–6Y– x Zn–0.6Zr magnesium alloys were prepared in an electromagnetic induction furnace under the protection of an Ar atmosphere. Table 1 lists the actual chemical composition of the designed alloys.

The microstructures of the specimens were examined by an Olympus optical microscope. Phase analysis was performed by a Rigaku D/MAX2500PC

Table 1 Chemical composition of Mg–9Er–6Y– x Zn–0.6Zr alloys (mass fraction)

Alloy No.	Nominal composition	Actual composition/%				
		Er	Y	Zn	Zr	Mg
I	Mg–9Er–6Y–1Zn–0.6Zr	8.89	5.73	0.77	0.68	Bal.
II	Mg–9Er–6Y–2Zn–0.6Zr	9.13	5.69	1.93	0.80	Bal.
III	Mg–9Er–6Y–3Zn–0.6Zr	9.13	5.67	3.05	0.71	Bal.
IV	Mg–9Er–6Y–4Zn–0.6Zr	9.03	5.74	4.27	0.80	Bal.

X-ray diffractometer using a copper target. The scanning angle was 20° – 80° , and the scanning speed was $2(^{\circ})/\text{min}$. The microstructural morphologies and compound compositions were determined by a VEGA ILMU scanning electron microscope with an energy dispersive X-ray spectrometer. The detailed microstructures of the samples were further examined under a TEM (Zeiss Libra 200 FE) operated at an accelerating voltage of 200 kV.

3 Results and discussion

Figure 1 shows the optical micrographs of the as-cast Mg–9Er–6Y– x Zn–0.6Zr alloys (I–IV) with different Zn contents. With increased Zn content, though the grain sizes of all four alloys did not present essential difference, yet, the second phases in the grain boundaries and grain interior had an obvious variation. In alloy I, numerous black granular precipitates with different sizes were generated in a discontinuous network mainly along the grain boundaries. Some lamellar phases grew parallel with each other from the grain boundaries to the grain interior. The morphology and distribution of the black

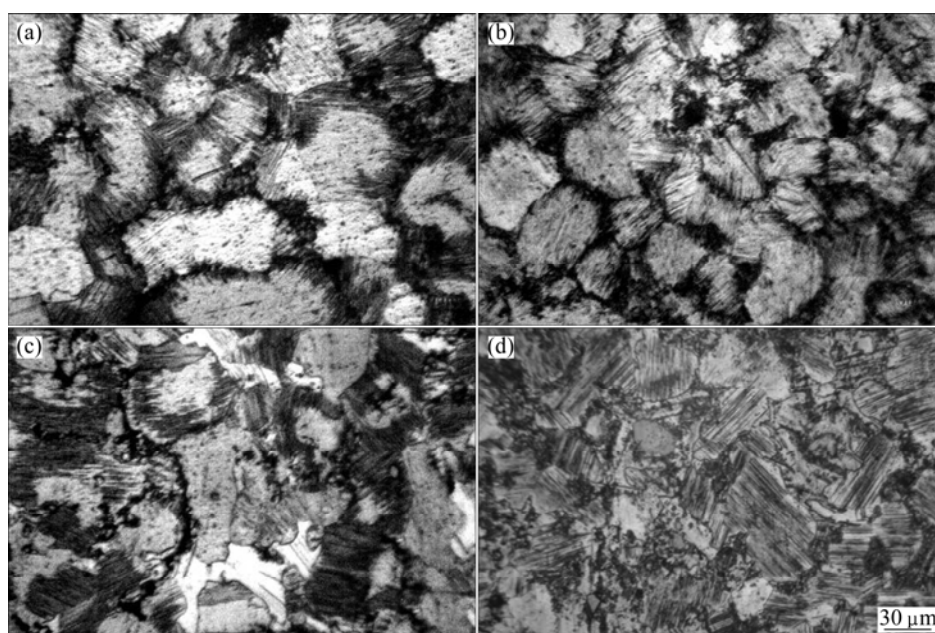


Fig. 1 Optical micrographs of as-cast Mg–9Er–6Y– x Zn–0.6Zr series alloys: (a) Alloy I; (b) Alloy II; (c) Alloy III; (d) Alloy IV

granular precipitates and lamellar phases in alloy II had no obvious difference from those of alloy I, except the finer crystal grains. With increased Zn content, the number of the granular black precipitates in alloys III and IV decreased. The precipitates were distributed in a more scattered manner, but mainly remained along the grain boundaries. Some other bright bulk-shaped precipitates emerged along the grain boundaries. Furthermore, the number of lamellar phases in the grain interior increased from alloys III to IV. A few matrix grains were penetrated thoroughly by the lamellar phases in alloy III. In alloy IV, the lamellar phases penetrating thoroughly the grains became much thicker distinctly.

In Mg–Er–Zn alloys, the effects of trace Er addition on their microstructures and phase compositions have already been researched. The $(\text{Mg,Zn})_4\text{Er}$ phases in as-cast Mg–1.5Zn–0.6Zr containing 0.5%, 1%, 2%, and 4% Er alloys have been identified by XRD patterns [15]. LI et al [17] have determined that $(\text{Mg,Zn})_4\text{Er}$ is iso-structural with $(\text{Mg,Zn})_4\text{Ho}$. Hexagonal $(\text{Mg,Zn})_4\text{RE}$ phases have also been found in RE=Y, Sm, Gd, Dy, and Yb cases. These phases are probably also iso-structural with $(\text{Mg,Zn})_4\text{Ho/Er}$. This structure is icosahedrally closely related to $\text{Mg}_3\text{Zn}_6\text{Y/Sm/Gd}$ [18,19] and MgZn_3Y [20]. All these three hexagonal phases coexist with icosahedral quasi-crystals in Mg–Zn–RE alloys. In as-cast Mg–5Zn–2.5Er alloy, the *I*-phase phase with an average stoichiometric composition of $\text{Mg}_{30}\text{Zn}_{60}\text{Er}_{10}$ is $\text{Mg}_{30.02}\text{Zn}_{58.94}\text{Er}_{11.04}$ (mole fraction, %). A face-centered icosahedral quasi-crystalline structure has also been detected and analyzed by EDS as well as selected area electron diffraction (SAED) [13].

However, studies on the microstructure and phase composition of Mg–Er–Y–Zn–Zr alloys with Er element as the major alloying element are almost non-existent. In Mg–Gd–Y–Zn–Zr alloys with Y as the major alloying element, $\text{Mg}_{24}(\text{Y,Gd,Zn})_5$ is the main second phase [4,21,22]. In Mg–Er binary alloys, $\text{Mg}_{24}\text{Er}_5$ acts as the eutectic phase [23,24]. Therefore, based on the XRD patterns shown in Fig. 2 and in previous literature, the main phase compositions in as-cast Mg–9Er–6Y–*x*Zn–0.6Zr alloys were α -Mg matrix, $\text{Mg}_{24}(\text{Er,Y,Zn})_5$, and $\text{Mg}_{12}\text{Zn}(\text{Y,Er})$. The XRD patterns of the as-cast alloys in Fig. 3 also reveal that α -Mg and $\text{Mg}_{24}(\text{Er,Y,Zn})_5$ phases with a little $\text{Mg}_{12}\text{Zn}(\text{Y,Er})$ phase existed in alloy I. However, with increased Zn content, both the number and intensity of the $\text{Mg}_{12}\text{Zn}(\text{Y,Er})$ phase diffraction peaks increased. In contrast, those of the $\text{Mg}_{24}(\text{Er,Y,Zn})_5$ phase decreased. This result indicated that the volume fraction of the $\text{Mg}_{12}\text{Zn}(\text{Y,Er})$ phase increased, whereas that of the $\text{Mg}_{24}(\text{Er,Y,Zn})_5$ phase decreased. In the $\text{Mg}_{12}\text{Zn}(\text{Y,Er})$ phase, the major formation atom was Zn. In the $\text{Mg}_{24}(\text{Er,Y,Zn})_5$ phase, the atoms of Er and Y were the major formation atoms, but Zn acted as the

substituted atom. Hence, the increased Zn content promoted the formation of the $\text{Mg}_{12}\text{Zn}(\text{Y,Er})$ phase, and restrained the generation of the $\text{Mg}_{24}(\text{Er,Y,Zn})_5$ phase. Subsequently, further confirmation of the secondary phases in the as-cast Mg–9Er–6Y–*x*Zn–0.6Zr alloys was performed via EDS.

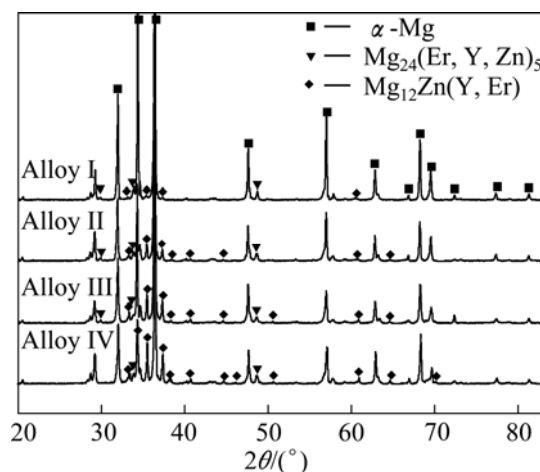


Fig. 2 XRD patterns of as-cast Mg–9Er–6Y–*x*Zn–0.6Zr alloys

The EDS test points and the corresponding results of the main phases in the as-cast Mg–9Er–6Y–*x*Zn–0.6Zr alloys are shown in Fig. 3 and Table 2. Test points *A*, *C*, *F*, and *I* in the Mg matrix show that only Y and Er served as the major solid solution atoms with a few Zn atoms. Figure 3 indicates that there were abundant bright granular phases distributed in the gray bulky phases, with a few of bright needle-like phases scattering among the bright granular phases in alloys, particularly as shown in Fig. 3(c). The EDS results of the second phases were not consistent with each other given their varied sizes in alloys I–IV. However, a concordant regularity was shown in terms of the bright granular phases and needle-like phases with lower Zn content as well as relatively high Y and Er contents. Zn served as the substitution atoms of Er and Y. Er and Y also served as the major formation atoms in the $\text{Mg}_{24}(\text{Er,Y,Zn})_5$ phase. Consequently, the average Mg/(Er,Y,Zn) mole ratio of the bright granular phases was 4.9, which was consistent with the Mg/(Er,Y,Zn) mole ratio of 4.8 in $\text{Mg}_{24}(\text{Er,Y,Zn})_5$. Therefore, the bright granular phase was the $\text{Mg}_{24}(\text{Er,Y,Zn})_5$ phase, as inferred from Figs. 2 and 3.

On the other hand, there was no evident gray bulky phase in alloy I (Figs. 2(a) and 4(a)). However, with 2% Zn (nominal composition), there were a few gray bulky phases that emerged in alloy II (Fig. 4(b)). The EDS results of the gray bulky phases in alloys II–IV show their approximately consistent stoichiometric compositions. These findings demonstrated a conspicuously different regularity in which the bright

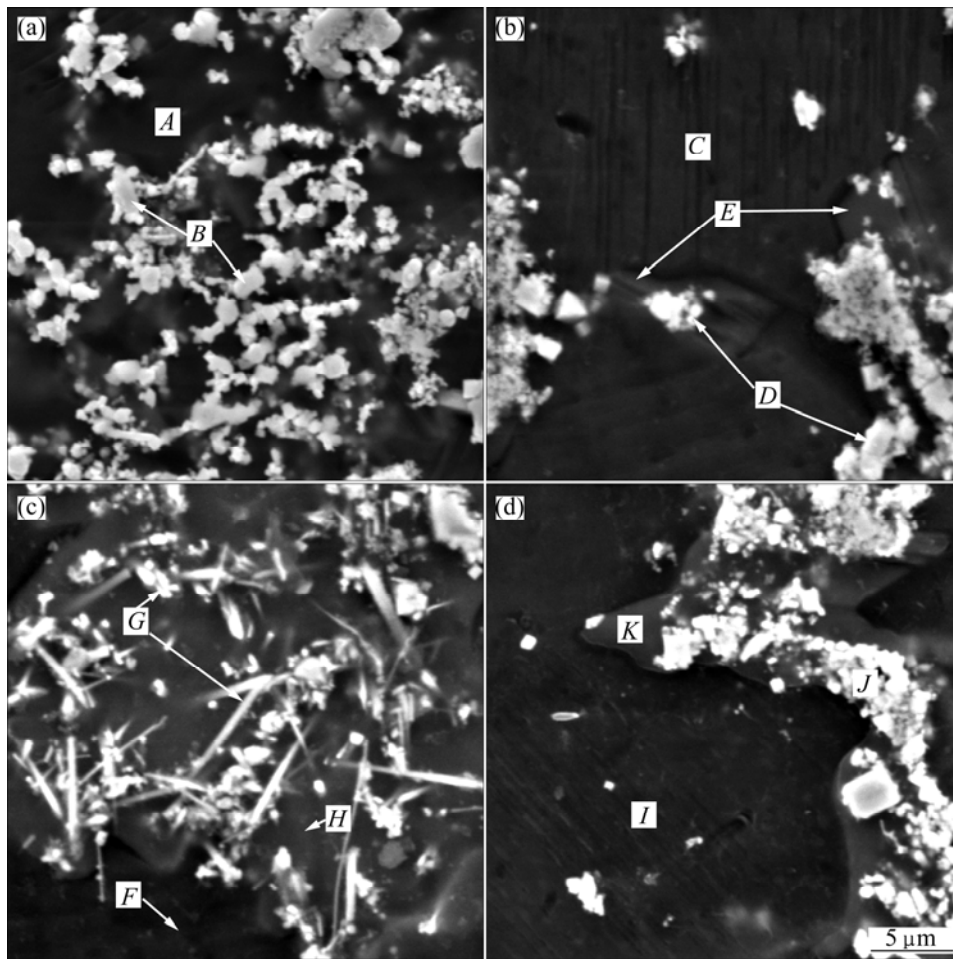


Fig. 3 SEM images and EDS analysis of as-cast Mg-9Er-6Y-*x*Zn-0.6Zr alloys: (a) Alloy I; (b) Alloy II; (c) Alloy III; (d) Alloy IV

Table 2 Corresponding EDS results of points in Fig. 3 for main phases in as-cast Mg-9Er-6Y-*x*Zn-0.6Zr alloys

Alloy No.	Main phase (Test point)	<i>x</i> (Mg)/%	<i>x</i> (Er)/%	<i>x</i> (Y)/%	<i>x</i> (Zn)/%
I	α -Mg matrix (A),	95.83	1.28	1.71	0.24
	bright granular phase (B)	82.86	6.59	8.27	2.28
II	α -Mg matrix (C),	95.52	1.46	1.73	0.16
	bright granular phase (D),	83.28	7.53	7.66	1.52
	gray bulky phase (E)	88.41	2.71	4.92	3.97
III	α -Mg matrix (F),	96.87	1.30	1.57	0.26
	bright granular phase (G),	82.93	6.66	6.83	3.57
	gray bulky phase (H)	84.68	3.72	5.68	5.92
IV	α -Mg matrix (I),	97.13	1.19	1.53	0.16
	bright granular phase (J),	82.86	6.05	5.76	5.34
	gray bulky phase (K)	86.56	3.07	4.88	5.50

granular phases had a lower Er content as well as higher Zn and Y contents than the bright granular phases. The Er atoms acted as substitution of the Y atoms; the Zn and Y atoms served as the major formation atoms in the $Mg_{12}Zn(Y,Er)$ phase. In addition, the average Mg/(Er,Y,Zn) mole ratio of the gray bulky phases was 6.5, which was consistent with the Mg/(Er,Y,Zn) mole ratio of 6 in $Mg_{12}Zn(Y,Er)$. Therefore, the gray bulky phase was the $Mg_{12}Zn(Y,Er)$ phase, as inferred from Figs. 2 and 3. Some previous studies have already reported that $Mg_{12}ZnRE$ phases possess the 14H-LPSO structure that is thermodynamically stable and in apparent equilibrium [8], which has an atomic composition of $Mg_{12}ZnY$, and is identical to that of the equilibrium $X-Mg_{12}ZnY$ phase in the Mg-Zn-Y system [25,26]. In the Mg-Gd-Y-Zn-Zr system, the LPSO phase also appears at the grain boundaries of Mg-10Gd-3Y-1.8Zn-0.4Zr alloys. The SAED pattern of these alloys show that they also have a LPSO structure ($a=0.3375$ nm and $c=3.5810$ nm). Their EDS spectra indicate that the LPSO phase has an average composition of $(88\pm 3)Mg-(4.5\pm 2)Gd-(1.5\pm 1)Y-(6\pm 2)Zn$ (mole fraction, %), i.e., $Mg_{12}Zn(Y,Gd)$ [27]. Moreover, in both Mg-Zn-Y and Mg-Zn-Er alloys, the

LPSO phase forms along grain boundaries as a secondary phase during solidification [11,12]. Hence, combining the results from the XRD patterns, SEM and EDS with the previous studies in Mg–RE–Zn–Zr series alloys mentioned above, it can be inferred that the gray bulky $\text{Mg}_{12}\text{Zn}(\text{Y},\text{Er})$ phase appearing at the grain boundaries is also a LPSO structure phase in the as-cast Mg–9Er–6Y–xZn–0.6Zr alloys. Subsequently, the crystallography structure for the $\text{Mg}_{24}(\text{Er},\text{Y},\text{Zn})_5$ phase and $\text{Mg}_{12}\text{Zn}(\text{Y},\text{Er})$ phase in the Mg–9Er–6Y–xZn–0.6Zr alloys was further confirmed by TEM.

Figure 4(a) shows the bright-field TEM image of the $\text{Mg}_{12}\text{Zn}(\text{Y},\text{Er})$ phase in alloy I. Moreover, the corresponding SAED patterns recorded along the $[1\bar{1}00]$ and $[11\bar{2}0]$ directions for the regions marked in Fig. 4 (a) are shown in Figs. 4 (b) and 4 (c), respectively. The SAED patterns shown in Figs. 4(b) and 4(c) illustrate weaker spots at position $n/6$ (where n is an integer) of the (0002) diffraction, which are evidences commonly used in previous studies [12,28,29] to prove the existence of the 18R-type LPSO structure. Five sets of weak streaks parallel to $(0\ 0\ 0\ 1)_\alpha$ direction at $\pm 1/6\{1120\}_\alpha$, $\pm 2/6\{1120\}_\alpha$, $\pm 3/6\{1120\}_\alpha$, $\pm 4/6\{1120\}_\alpha$, and $\pm 5/6\{1120\}_\alpha$ positions can be observed in Fig. 4(b). Moreover, the SAED pattern in Fig. 4(c) was supposed to show two very weak streaks parallel to the $(0\ 0\ 0\ 1)_\alpha$ direction at the $\pm 1/2[1\bar{1}00]_\alpha$ position. However, these streaks are not shown clearly, probably because their intensities are too low to be readily detectable with the

normal exposure time employed. As confirmed by ABE et al [6], these streaks may be related to the periodical enrichment of Y and Zn atoms on particular close-packed planes in the LPSO phases. The analyses of these diffraction patterns indicates that this 18R LPSO phase has a hexagonal structure with lattice parameters $a=0.31\text{ nm}$ and $c=4.44\text{ nm}$ (Note that, for the sake of simplicity, the 18R crystal structure was indexed by hexagonal notation in the present study by considering the unit cell to be three times larger than the rhombohedral cell [30]). In addition, previous studies demonstrated the stacking sequence $ABABABCACAC-ABCBCBC$ of the 18R-type LPSO phase using high-resolution TEM [7, 30, 31].

The bright-field TEM image of the $\text{Mg}_{24}(\text{Er},\text{Y},\text{Zn})_5$ phase in alloy I is shown in Fig. 4(d). In addition, the corresponding SAED patterns recorded along the $[011]$ direction for the $\text{Mg}_{24}(\text{Er},\text{Y},\text{Zn})_5$ phases marked in Fig. 4(d) are shown in Fig. 4(e). The analyses of these diffraction patterns indicate that this phase has a body-centred cubic structure with a lattice parameter of $a=10.66\text{ \AA}$. A previous study [23] on the phase equilibrium in the erbium–magnesium system hypothesized that $\text{Mg}_{24}\text{Er}_5$ has a cubic crystallography structure, belonging to the $cI58-\alpha\text{Mn}$ type with a lattice parameter of $a=11.214\text{ \AA}$, which is approximately coincident with our results.

Except for the main second phases, i.e., $\text{Mg}_{24}(\text{Er},\text{Y},\text{Zn})_5$ and $\text{Mg}_{12}\text{Zn}(\text{Y},\text{Er})$, distributed in the

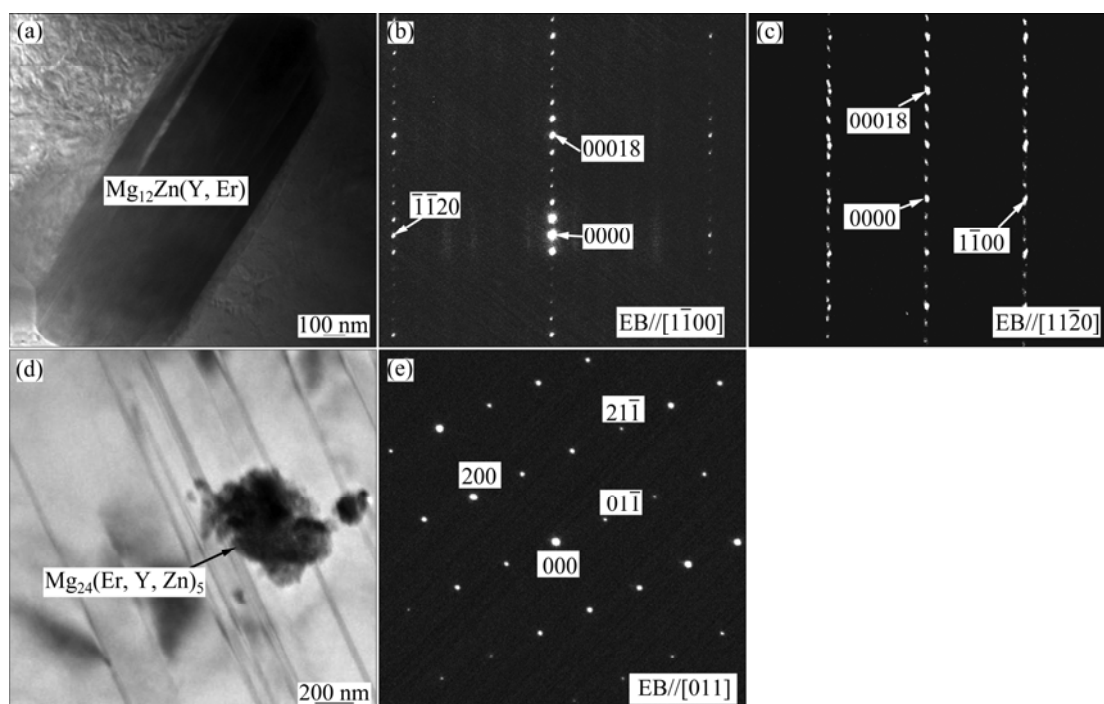


Fig. 4 Bright-field TEM image of $\text{Mg}_{12}\text{Zn}(\text{Y},\text{Er})$ phase (a) and its corresponding SAED pattern recorded along $[1\bar{1}00]_\alpha$ direction (b) and $[11\bar{2}0]_\alpha$ direction (c), bright-field TEM image of $\text{Mg}_{24}(\text{Er},\text{Y},\text{Zn})_5$ phase (d) and its corresponding SAED pattern recorded along $[011]$ direction (e) in alloy I

grain boundaries, some other lamellar phases grew parallel with each other from the grain boundaries to the grain interior in alloys I–IV. These lamellar phases had different orientations in different grains, indicating that they had a certain crystallographic orientation relationship with the α -Mg matrix. This finding is also commonly observed in other as-cast Mg–Gd–Y–Zn–Zr alloys. The effects of different cooling rates on Mg–10Gd–3Y–1.8Zn–0.4Zr alloys have indicated [28] that a fine lamellar LPSO structure appears in the matrix near grain boundaries at a cooling rate of 5 K/s. With decreasing cooling rate, the lamellar LPSO structure propagates in the α -Mg matrix. With a very slow cooling rate (0.005 K/s), the lamellar LPSO structure penetrates throughout the matrix grain. These Mg–9Er–6Y– x Zn–0.6Zr alloys were prepared in an electromagnetic induction furnace, and solidified at ambient air at an approximate cooling rate of 0.01 K/s. The microstructures of the as-cast alloys presented the lamellar phases in the α -Mg matrix grains near the grain boundaries, corresponding to those in the previous reports. Therefore, it can be inferred that the lamellar phases in the as-cast Mg–9Er–6Y– x Zn–0.6Zr alloys also have the LPSO iso-structure determined in the as-cast Mg–Gd–Y–Zn–Zr alloys. However, under the same cooling rate, the number of the lamellar phases in alloys I–IV increased with increasing Zn content (Fig. 1). The formation of the LPSO structure needed the Zn atoms with a relatively high diffusion rate to diffuse into the Mg matrix, and generate the lattice distortion or defect. The purpose was to provide the space where the RE atoms can diffuse into the matrix, and sequentially generate the stacking fault. Given enough Zn and RE atoms and diffusion time, the unordered stacking fault can transform into the LPSO structure. Therefore, the increased content of Zn atoms, which acted as the essential formation atoms in the LPSO structure phases, not only promoted the generation of block LPSO phases in the grain boundaries, but also induced the propagation of the LPSO structure lamellar phases in the as-cast alloys. The phase compositions of the as-cast Mg–9Er–6Y– x Zn–0.6Zr alloys are summarized and listed in Table 3.

Table 3 Phase compositions of as-cast Mg–9Er–6Y– x Zn–0.6Zr series alloys

Alloy No.	$x(\text{Zn}/(\text{Gd}+\text{Y}))/\%$	Phase composition
I	0.1	α -Mg, Mg ₂₄ (Er,Y,Zn) ₅ and lamellar phase
II	0.25	α -Mg, Mg ₂₄ (Er,Y,Zn) ₅ Mg ₁₂ Zn(Y,Er), and lamellar phase
III	0.40	α -Mg, Mg ₂₄ (Er,Y,Zn) ₅ Mg ₁₂ Zn(Y,Er), and lamellar phase
IV	0.55	α -Mg, Mg ₂₄ (Er,Y,Zn) ₅ Mg ₁₂ Zn(Y,Er), and lamellar phase

4 Conclusions

1) With increasing Zn, the Mg₂₄(Er,Y,Zn)₅ phases decreases, and the lamellar as well as Mg₁₂Zn(Y,Er) phases continuously increases. When the content of Zn reaches 3% (normal composition), the Mg₁₂Zn(Y,Er) phases mainly exist as large bulks, and some α -Mg grains are thoroughly penetrated by the lamellar phases.

2) The crystallography structure of the Mg₁₂Zn(Y,Er) and Mg₂₄(Er,Y,Zn)₅ phases are confirmed as 18R-type long-period stacking ordered structure and body-centred cubic structure, respectively.

References

- [1] ANYANWU I A, KAMADO S, KOJIMA Y. Platform science and technology for advanced magnesium alloys. Creep properties of Mg–Gd–Y–Zr alloys [J]. Materials Transactions JIM, 2001, 42: 1212–1218.
- [2] ROKHLIN L L. Magnesium alloys containing rear earth metals: Structure and properties [C]//Advances in Metallic Alloys Series. London: Taylor and Francis Group, 2003.
- [3] HONMA T, OHKUBO T, KAMADO S, HONO K. Effect of Zn additions on the age-hardening of Mg–2.0Gd–1.2Y–0.2Zr alloys [J]. Acta Materialia, 2007, 55: 4137–4150.
- [4] LIU K, ROKHLIN L L, ELKIN F M, TANG D X, MENG J. Effect of ageing treatment on the microstructures and mechanical properties of the extruded Mg–7Y–4Gd–1.5Zn–0.4Zr alloy [J]. Materials Science and Engineering A, 2010, 527: 828–834.
- [5] KAWAMURA Y, HAYASHI K, INOUE A, MASUMOTO T. Rapidly solidified powder metallurgy Mg₉₇Zn₁Y₂ alloys with excellent tensile yield strength above 600 MPa [J]. Materials Transactions JIM, 2001, 42: 1172–1176.
- [6] ABE E, KAWAMURA Y, HAYASHI K, INOUE A. Long-period ordered structure in a high-strength nanocrystalline Mg–1at% Zn–2at% Y alloy studied by atomic-resolution Z-contrast STEM [J]. Acta Materialia, 2002, 50: 3845–3857.
- [7] MATSUDA M, LI S, KAWAMURA Y, IKUHARA Y, NISHIDA M. Variation of long-period stacking order structures in rapidly solidified Mg₉₇Zn₁Y₂ alloy [J]. Materials Science and Engineering A, 2005, 393: 269–274.
- [8] ZHU Y M, MORTON A J, NIE J F. The 18R and 14H long-period stacking ordered structures in Mg–Y–Zn alloys [J]. Acta Materialia, 2010, 58: 2936–2947.
- [9] YANG Z, LI J P, GUO Y C, LIU T, XIA F, ZENG Z W, LIANG M X. Precipitation process and effect on mechanical properties of Mg–9Gd–3Y–0.6Zn–0.5Zr alloy [J]. Materials Science and Engineering A, 2007, 454–455: 274–280.
- [10] HOMMA T, KUNITO N, KAMADO S. Fabrication of extraordinary high-strength magnesium alloy by hot extrusion [J]. Scripta Materialia, 2009, 61: 644–647.
- [11] ITOI T, SEIMIYA T, KAWAMURA Y, HIROHASHI M. Long period stacking structures observed in Mg₉₇Zn₁Y₂ alloy [J]. Scripta Materialia, 2004, 51: 107–111.
- [12] YOSHIMOTO S, YAMASAKI M, KAWAMURA Y. Microstructure and mechanical properties of extruded Mg–Zn–Y alloys with 14H long period ordered structure [J]. Materials Transactions, 2006, 47: 959–965.

- [13] LI J H, DU W B, LI S B, WANG Z H. Icosahedral quasicrystalline phase in an as-cast Mg–Zn–Er alloy [J]. *Rare Metals*, 2009, 28(3): 297–301.
- [14] LI J H, DU W B, LI S B, WANG Z H. Precipitation behavior of the Mg–Zn–Er alloy reinforced by the icosahedral quasicrystal [J]. *Rare Metals*, 2009, 28: 261–264.
- [15] ZHANG J, ZHANG X F, LI W G, PAN F S, GUO Z X. Partition of Er among the constituent phases and the yield phenomenon in a semi-continuously cast Mg–Zn–Zr alloy [J]. *Scripta Materialia*, 2010, 63: 367–370.
- [16] ZHANG J, LI W G, ZHANG B X, DOU Y C. Influence of Er addition and extrusion temperature on the microstructure and mechanical properties of a Mg–Zn–Zr magnesium alloy [J]. *Materials Science and Engineering A*, 2011, 528: 4740–4746.
- [17] LI M R, DENG D W, KUO K H. Crystal structure of the hexagonal (Zn, Mg)₄Ho and (Zn, Mg)₄Er [J]. *Journal of Alloys and Compounds*, 2006, 414: 66–72.
- [18] TAKAKURA H, SATO A, YAMAMOTO A, TSAI A P. Crystal structure of a hexagonal phase and its relation to a quasicrystalline phase in Zn–Mg–Y alloy [J]. *Philosophical Magazine Letters*, 1998, 78: 263–270.
- [19] SUGIYAMA K, YASUDA K, OHSUNA T, HIRAGA K. The structures of hexagonal phases in Mg–Zn–RE (RE=Sm and Gd) alloys [J]. *Zeitschrift Für Kristallographie*, 1998, 213: 537–543.
- [20] DENG D W, KUO K H, LUO Z P, MILLER D J, KRAMER M J, DENNIS D W. Crystal structure of the hexagonal Zn₃MgY phase [J]. *Journal of Alloys and Compounds*, 2004, 373: 156–160.
- [21] GAO Y, WANG Q D, GU J H, ZHAO Y, TONG Y, YIN D D. Comparison of microstructure in Mg–10Y–5Gd–0.5Zr and Mg–10–Y–5Gd–2Zn–0.5Zr alloys by conventional casting [J]. *Journal of Alloys and Compounds*, 2009, 477: 374–378.
- [22] LIU K, J H ZHANG, SU G H, TANG D X, ROKHLIN L L, ELKIN F M, MENG J. Influence of Zn content on the microstructure and mechanical properties of extruded Mg–5Y–4Gd–0.4 Zr alloy [J]. *Journal of Alloys and Compounds*, 2009, 481: 811–818.
- [23] SACCONI A, DELFINO S, MACCIO D, FERRO R. Phase equilibria in the binary rare-earth alloys: The erbium–magnesium system [J]. *Metallurgical and Materials Transactions A*, 1992, 23: 1005–1012.
- [24] OKAMOTO H. Desk handbook: Phase diagrams for binary alloys [M]. America: ASM International, 2000.
- [25] PADEZHNOVA E M, MEL'NIK E V, MILIYEVSKIY R A, DOBATKINA T V, KINZHIBALOV V V. Investigation of the Mg–Zn–Y system [J]. *Russian Metallurgy (Metally)*, 1982, 4: 185–188.
- [26] SHAO G, VARSANI V, FAN Z. Thermodynamic modelling of the Y–Zn and Mg–Zn–Y systems [J]. *Computer Coupling of Phase Diagrams and Thermo-chemistry*, 2006, 30: 286–295.
- [27] ZHANG S, YUAN G Y, LU C, DING W J. The relationship between (Mg,Zn)₃RE phase and 14H-LPSO phase in Mg–Gd–Y–Zn–Zr alloys solidified at different cooling rates [J]. *Journal of Alloys and Compounds*, 2011, 509: 3515–3521.
- [28] KLYAMKIN S N, KANDALOVA N V, VERBETSKII V N, SEMENENKO K N. The synthesis of ternary hydrides in the Mg–Yb–H₂ and Mg–Er–H₂ systems [J]. *Russian Journal of Inorganic Chemistry*, 1991, 36: 122–124.
- [29] YAMASAKI M, ANAN T, YOSHIMOTO S, KAWAMURA Y. Mechanical properties of warm-extruded Mg–Zn–Gd alloy with coherent 14H long periodic stacking ordered structure precipitate [J]. *Scripta Materialia* 2005, 53: 799–803.
- [30] HAGIHARA K, YOKOTANI N, UMAKOSHI Y. Plastic deformation behavior of Mg₁₂YZn with 18R long-period stacking ordered structure [J]. *Intermetallics*, 2010, 18: 267–276.
- [31] SHAO X H, YANG Z Q, MA X L. Strengthening and toughening mechanisms in Mg–Zn–Y alloy with a long period stacking ordered structure [J]. *Acta Materialia*, 2010, 58: 4760–4771.

铸态 Mg–9Er–6Y–xZn–0.6Zr 合金的显微组织及相组成

王敬丰^{1,2}, 宋鹏飞¹, 潘复生^{1,2}, 周小蓊¹

1. 重庆大学 材料科学与工程学院, 重庆 400044;

2. 重庆大学 国家镁合金材料工程技术研究中心, 重庆 400044

摘要: 对铸态 Mg–9Er–6Y–xZn–0.6Zr (x=1, 2, 3, 4; 名义质量分数) 系列合金的显微组织和相组成进行了研究。在低 Zn 含量的合金中, 第二相主要以 Mg₂₄(Er,Y,Zn)₅ 存在, 除此之外, 在 α-Mg 基体中出现了一些从晶界向晶粒内部平行生长的层状相。随着 Zn 含量的增加, Mg₂₄(Er,Y,Zn)₅ 相不断减少, 而 Mg₁₂Zn(Y,Er) 相和层状相不断增多。当合金中 Zn 含量达到 4% (名义成分) 时, Mg₁₂Zn(Y,Er) 相主要以大块状形貌存在, 而部分 α-Mg 基体中的层状相已几乎贯穿了部分晶粒。此外, Mg₁₂Zn(Y,Er) 和 Mg₂₄(Er,Y,Zn)₅ 相的晶体结构被分别确定为 18R 型的长周期堆垛有序结构和体心立方结构。

关键词: 镁合金; 显微组织; 相组成; 长周期堆垛有序(LPSO)相

(Edited by Xiang-qun LI)